ASTROBIOLOGY
Volume 18, Number 8, 2018

DOI: 10.1089/ast.2017.1757

A Complex Fluviolacustrine Environment on Early Mars and Its Astrobiological Potentials

Jun Huang (黄俊),[1,2,5] Mark R. Salvatore,[3] Christopher S. Edwards,[3] Rachel L. Harris,[4] and Philip R. Christensen[5]

Abstract

Chloride-bearing deposits and phyllosilicates-bearing units are widely distributed in the southern highlands of Mars, but these phases are rarely found together in fluviolacustrine environments. The study of the coexistence of these minerals can provide important insights into geochemistry, water activity, and ultimately the climate and habitability of early Mars. Here we use high-resolution compositional and morphological orbiter data to identify and characterize the context of diverse minerals in a Noachian fluviolacustrine environment west of Knobel crater (6.7°S, 226.8°W). The chlorides in this region are likely formed through the evaporation of brines in a closed topographic basin. The formation age of chlorides is older than 3.7 Ga, based on stratigraphic relationships identified and previously obtained crater retention ages. The timing of the alteration of basaltic materials to iron–magnesium smectites in relation to the chloride formation in this location is enigmatic and is unable to be resolved with currently available remote sensing data. Importantly, we find that this close relationship between these key minerals revealed by the currently available data details a complex and intimate history of aqueous activity in the region. Of critical importance are the evaporitic deposits as analogous terrestrial deposits have been shown to preserve ancient biosignatures and possibly even sustain microbial communities for hundreds of millions of years. These salts could have protected organic matter from ultraviolet radiation, or even allow modern habitable microenvironments in the shallow subsurface through periodic deliquescence. The high astrobiology potential of this site makes it a good candidate for future landed and sample return missions (*e.g.*, the Chinese 2020 Mars mission).
Key Words: Chloride—Phyllosilicate—Astrobiology—Fluviolacustrine environment—China Mars Mission—Mars. Astrobiology 18, 1081–1091.

1. Introduction

Globally distributed chloride-bearing materials (chlorides) have been previously identified on Mars (Osterloo *et al.*, 2008) using spectral data from the Thermal Emission Imaging System (THEMIS) (Christensen *et al.*, 2004) and the Thermal Emission Spectrometer (TES) (Christensen *et al.*, 2001). The mid-infrared (IR) spectra of the chlorides exhibit a low emissivity over 8–12 μm and distinctive blue slope in TES and THEMIS data, whereas the visible/near-IR spectra of them show a featureless red slope over ~1–2.6 μm and positive 3 μm features in ratioed Compact Reconnaissance Imaging Spectrometer for Mars (CRISM) (Murchie *et al.*, 2007) data (Murchie *et al.*, 2009; Osterloo *et al.*, 2010; Ruesch *et al.*, 2012), indicating material that is less hydrated than typical martian surface material. Laboratory data show these chlorides can be matched by mixtures of 10–25% anhydrous chloride salts and silicates (Jensen and Glotch, 2011; Glotch *et al.*, 2016). Terrestrial sites analogous to these chloride deposits often host halophilic microorganisms and preserved organic matter (Farmer and Des Marais, 1999), which makes them targets of high astrobiological interest.

Sites with juxtaposed phyllosilicates and chlorides are of particular interest due to apparent lack of other major alteration phases (*e.g.*, carbonates and sulfates and phyllosilicates) associated with most chlorides. In these sites, phyllosilicates have typically been found to underlie chlorides (Glotch *et al.*,

[1]Planetary Science Institute, State Key Laboratory of Geological Processes and Mineral Resources, School of Earth Sciences, China University of Geosciences, Wuhan, China.
[2]Lunar and Planetary Science Laboratory, Macau University of Science and Technology–Partner Laboratory of Key Laboratory of Lunar and Deep Space Exploration, Chinese Academy of Sciences, Macau, China.
[3]Department of Physics and Astronomy, Northern Arizona University, Flagstaff, Arizona.
[4]Department of Geosciences, Princeton University, Princeton, New Jersey.
[5]School of Earth and Space Exploration, Arizona State University, Tempe, Arizona.

2010; Hynek *et al.*, 2015), strongly suggesting that these chlorides are younger than these other alteration phases.

Our investigation focuses on a topographically enclosed basin south of the dichotomy boundary and adjacent to the west rim of Knobel crater (near Gale crater) ~3000 km^2 in area centered near 6.078°S, 132.346°E (Fig. 1). Numerous channels of different lengths and degradation incise the surrounding highlands, and one major outlet channel (~300 m deep) dissects the northeastern segment of the basin and runs into Sharp crater. Knobel crater has a wrinkle-ridged flat floor that is made of volcanic materials, whereas Sharp crater has chaos terrains with a fully degraded northern rim and no apparent ejecta blanket (Ehlmann and Buz, 2015).

Here we identify the coexistence of chlorides and phyllosilicates in this basin using THEMIS and CRISM data. Coupled with high spatial resolution images from the High Resolution Imaging Science Experiment (HiRISE) (McEwen *et al.*, 2007) and Context Camera (CTX) (Malin *et al.*, 2007), we observe the complex stratigraphic relationship between chlorides and iron–magnesium smectite clays. This region appears to have a more complex geological history than other more stratigraphically simple phyllosilicate–chloride-bearing sites (Glotch *et al.*, 2010; Hynek *et al.*, 2015). These two compositionally distinct units in the study area represent unique events and diverse environments in a middle-Noachian (Tanaka *et al.*, 2014) fluviolacustrine environment.

The formation and evolution of a sedimentary deposit in this site are particularly interesting astrobiological implications. Evaporite deposits on Earth often provide good preservation conditions for organic matter up to hundreds of million years (Gemmell *et al.*, 1998; McGenity *et al.*, 2000; Vreeland *et al.*, 2000, 2007; Fish *et al.*, 2002; Stan-Lotter *et al.*, 2002; Ueno *et al.*, 2006; Schubert *et al.*, 2010; Saralov *et al.*, 2013). Although the chlorides are Noachian in age, we postulate that microscopic fluid inclusions may have persisted long after larger liquid water bodies were lost at the surface. To this end, we must consider that if life had been present on the martian surface during the Noachian, these fluid inclusions present one possibility in which life may have continued to survive, metabolize, and reproduce after the rest of the surface became comparatively inhospitable. Periodic deliquescence of local hygroscopic salts (Martín-Torres *et al.*, 2015) may have served

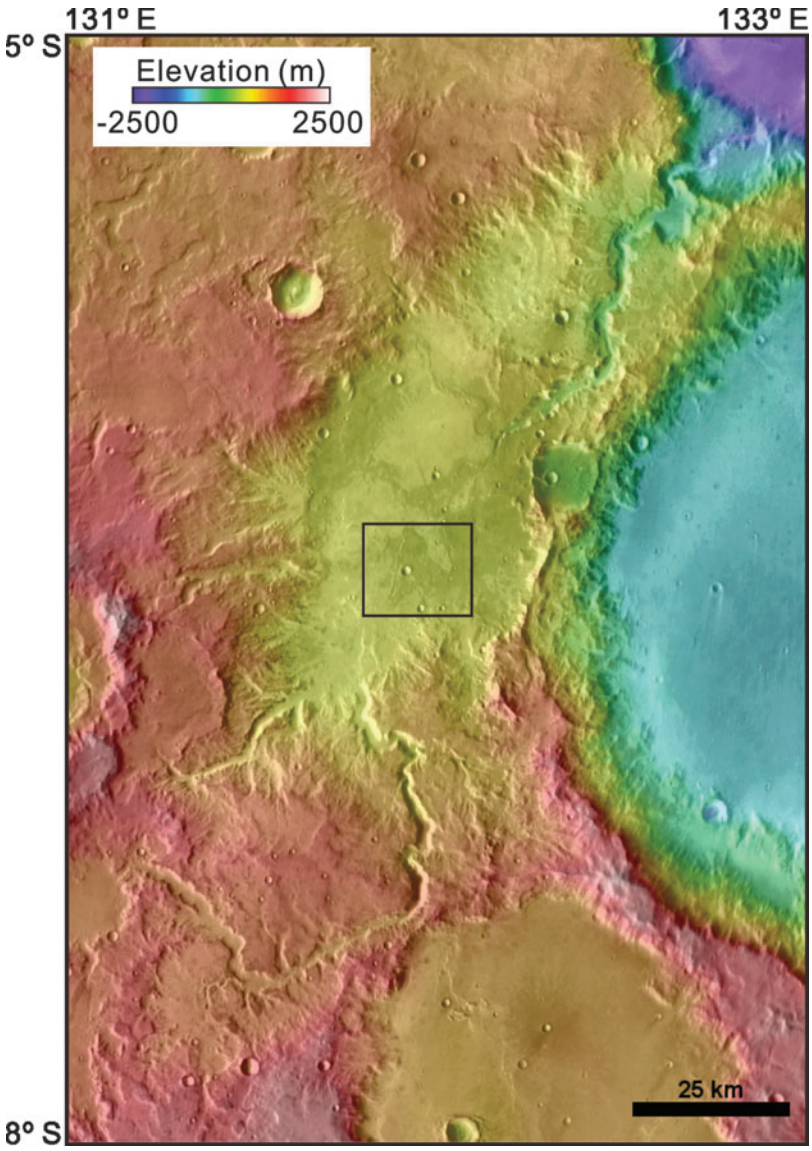

FIG. 1. Regional context of the study area: a ~3000 km^2 topographically enclosed basin. Numerous channels of different lengths and degradation incise the surrounding highlands, and one major outlet channel (~300 m deep) dissects the northeastern segment of the basin. It is colorized MOLA topography overlain on a THEMIS daytime IR mosaic. The rectangle shows the location of Figures 2a, 3a, b, and 4a. IR, infrared; THEMIS, Thermal Emission Imaging System.

as a means of nutrient recharge for these microenvironments to sustain *in situ* microbial communities for extended periods. In addition, smectite clays are notable for organic carbon sequestration and preservation (Kennedy, *et al.*, 2002; Ehlmann *et al.*, 2008). The juxtaposition of these minerals provides unique astrobiological prospects for long-term habitability and biosignature preservation potential at the microscopic scale. As such, this site should be considered as a potential site for future martian surface investigations (*e.g.*, the coming Chinese 2020 Mars rover).

2. Methods

The THEMIS instrument onboard the Mars Odyssey spacecraft acquires thermal IR images from 6.78 to 14.88 μm at 100 m/px in nine spectral bands centered at 6.78, 7.93, 8.56, 9.35, 10.21, 11.04, 11.79, 12.57, and 14.88 μm. The brightness temperature of the surface is calculated by fitting a Planck curve to band 9 (centered at 12.57 μm) calibrated radiance due to the highest signal-to-noise ratio and relative transparency to atmospheric dust at this band. This brightness temperature is a proxy of surface kinetic temperature, and the band 9 daytime IR global mosaic of THEMIS (Edwards *et al.*, 2011) highlights relative daytime surface temperatures of different geological materials. We used THEMIS radiance images corrected for instrument effects in Java Mission-planning and Analysis for Remote Sensing (JMARS; http://jmars.asu.edu) software to reconnaissance regional compositional variations (Bandfield *et al.*, 2004; Huang *et al.*, 2013). The occurrences of chlorides exhibit a unique blue hue (Osterloo *et al.*, 2008) in running decorrelation stretches (DCSs) on THEMIS day IR radiance images (Gillespie *et al.*, 1986; Edwards *et al.*, 2011). The unique blue hue is due to a spectral slope in homogeneously low emissivity in the wavelength of 6.78–14.88 μm of THEMIS day IR data. The spectral slope is an artifact of the assumption of an emissivity of 1, as chloride is a gray body and never has an emissivity of 1. We chose THEMIS day IR images acquired local early afternoon (relatively higher surface temperature and higher signal-to-noise value) and with lower atmospheric opacity to map the occurrences of chlorides in the study area. THEMIS IR images also measure nighttime surface temperatures, and the nighttime temperatures are calibrated to within a precision of 1.2K and absolute accuracy of $\sim$2.8K at night (at 180K). The THEMIS night IR images were used to model thermal inertia (Fergason *et al.*, 2006; Kieffer, 2013) due to the absence of effects of albedo and Sun-heated slopes and the maximum thermal contrast caused by different particle sizes. Thermal inertia is a fundamental material property and is defined as $I=(KRC)^{1/2}$, where K is thermal conductivity, R is equal to density, and C is equal to heat capacity. The thermal model originated from Viking IRTM thermal model (Kieffer *et al.*, 1977) is modified with the replacement of a constant atmospheric thermal radiation with a one layer that is spectrally gray at solar wavelengths, and the direct and diffuse illuminations are computed using a two-stream delta-Eddington model. The THEMIS band 9 temperatures are converted to a thermal inertia by interpolation within a look-up table, which is generated by selecting values appropriate for six input parameters: latitude, season, local solar time, atmospheric dust opacity, elevation (atmospheric pressure), and albedo (Fergason *et al.*, 2006). Higher thermal inertia materials are typically consistent with a larger effective grain size or well indurated, whereas low thermal inertia indicates fine particulate and unconsolidated particulate materials (Piqueux and Christensen, 2011). Surface exposures of rocks or ice exhibit high thermal inertia (*e.g.*, >1200 $Jm^{-2}K^{-1}s^{-0.5}$), whereas surface covered with relatively thick dust exhibits low thermal inertia (*e.g.*, <100 $Jm^{-2}K^{-1}s^{-0.5}$) (Mellon *et al.*, 2000; Putzig *et al.*, 2005; Edwards *et al.*, 2009). The thermal inertia data derived from THEMIS night IR images are also available in JMARS.

In addition to thermal data, we examined CRISM hyperspectral data to further constrain the composition of the materials in question. CRISM collects hyperspectral visible/near-IR images from 362 to 3920 nm at 6.55 nm/band and 18 m/px. We remove the atmospheric components within the CRISM full resolution targeted (FRT) data using a volcano-scan algorithm (McGuire *et al.*, 2009) through CRISM Analysis Tool (CAT; pds-geosciences.wustl.edu/missions/mro/crism.htm). We used the band combination proposed in Glotch *et al.* (2010) to highlight the composition variation in the FRT scene. Spectra were extracted and averaged from regions of interest, and divided by relatively spectrally featureless spectra of dusty regions to remove residual atmospheric components and identify chlorides, hydrated or iron-bearing phases, and low-calcium pyroxene (LCP).

In addition to composition data from THEIMS, TES, and CRISM, we relied on coregistered morphological data to help place constraints on the geological setting. The spatial sampling of CTX and HiRISE images is 6 m/px and 0.25 cm/px, respectively. These data were coupled with the compositional data sets to characterize the geomorphology and establish stratigraphic relationship of different geological units. We use stereo pairs of CTX (P20_008780_1727_XN_07S228W and G14_023588_1735_XI_06S228W) and HiRISE (PSP_008780_1735 and ESP_044502_1735) images to generate digital terrain models (DTMs with Ames Stereo Pipeline) (Shean *et al.*, 2016) for a small scale topographic study.

3. Results

We identified various geological units with complex stratigraphic relationships in the topographically enclosed basin. We observed a highly degraded fan deposit at the terminus of the two main inlet channels to the southwest (Fig. 2a). Possible layering exposed by an impact crater can be observed along the western side of an eroded fan structure (Fig. 2b), which may indicate multiple pulses or episodes of sedimentary deposition. Relatively light-toned materials can be seen throughout the study region: the largest occurrences in the northern part of the fan unit, and tens of smaller occurrences result in isolated ''geological windows'' (the lower stratigraphic units are visible through the ''holes'' of the upper stratigraphic units) (Fig. 2a). Collectively, these light-toned materials have elevated thermal inertia ($\sim$500 J K^{-1} m^{-2} $s^{-1/2}$) compared with adjacent materials ($\sim$200–300 J K^{-1} m^{-2} $s^{-1/2}$; Fig. 3a), and likely indicate they are composed of materials with larger grain sizes and/or are indurated/cemented (Piqueux and Christensen, 2011). These light-toned materials with elevated thermal inertias appear blue (Fig. 3b) in DCS images of THEMIS bands 8, 7, and 5, which is unique to chlorides (Osterloo *et al.*, 2008, 2010; Glotch *et al.*, 2010). As confirmed by DCSs of CRISM bands centered at 1.8, 2.38,

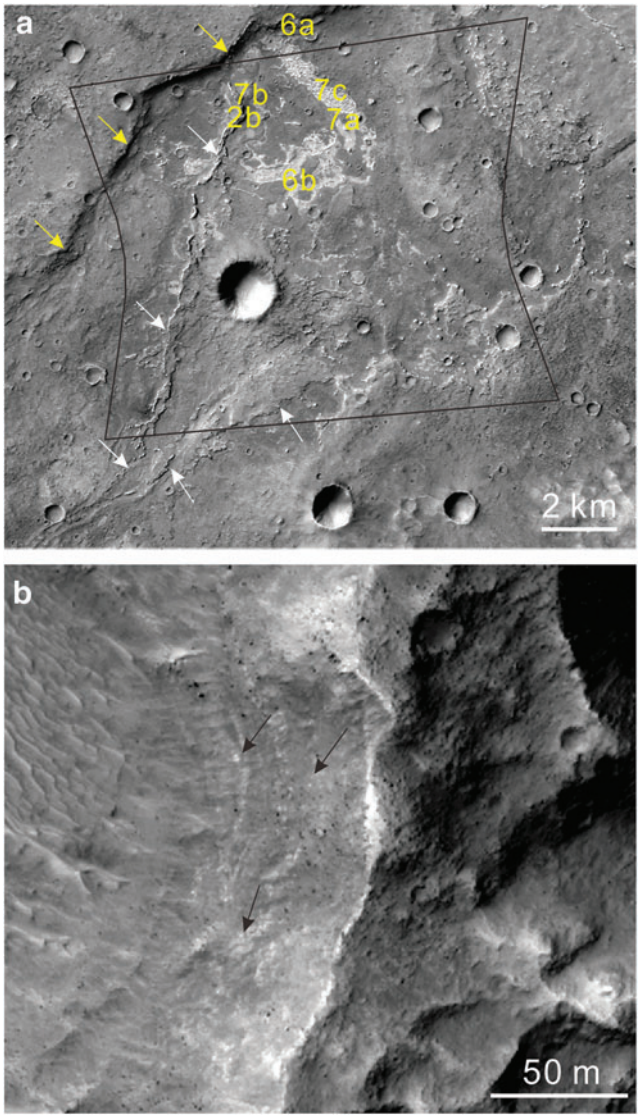

FIG. 2. **(a)** Close view of the lower portion of the basin, CTX image P20_008780_1727_XN_07S228W. The polygon shows the outline of Figure 4a. Labels show locations of Figures 2b, 6a, b, and 7a, b. The elevated ridges indicated by white arrows are possible remnants of an alluvial fan. The scarp separates the lower and higher floor of the basin and is indicated by yellow arrows. **(b)** Black arrows indicate layered deposits in the elevated ridges, indicating multiple fluvial activities. HiRISE PSP_008780_1735. CTX, Context Camera; HiRISE, High Resolution Imaging Science Experiment.

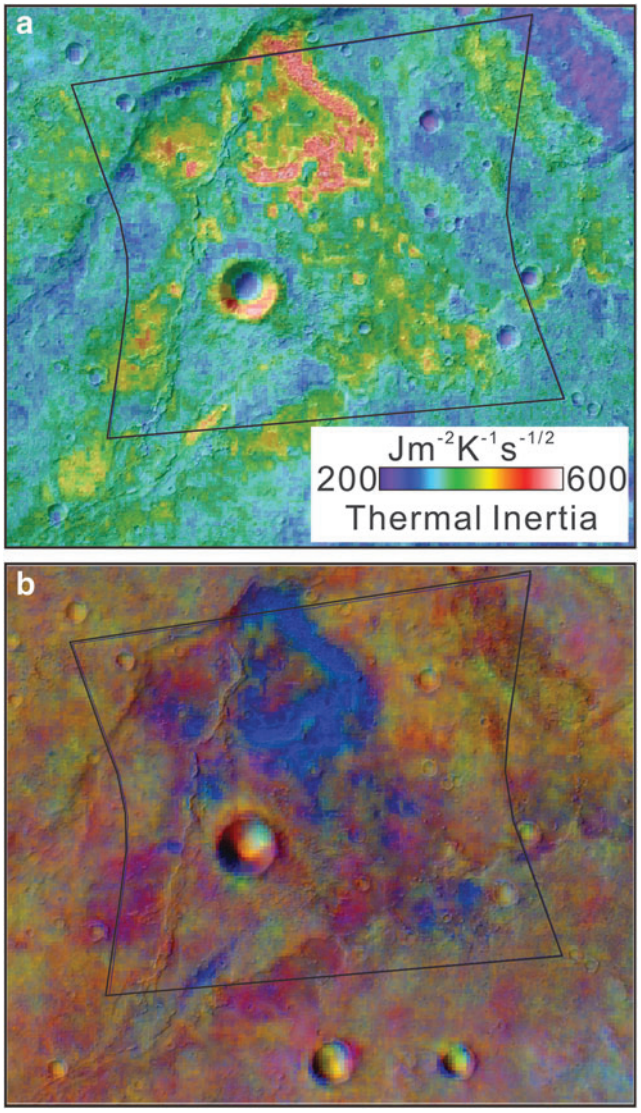

FIG. 3. **(a)** Colorized thermal inertia data derived from THEMIS nighttime IR image I05582005 overlain CTX image P20_008780_1727_XN_07S228W. **(b)** Bands 8, 7, and 5 DCS image of THEMIS daytime IR image I33779001 overlain CTX P20_008780_1727_XN_07S228W. Chlorides are in blue hue, which are within elevated thermal inertia units. The polygon shows the outline of Figure 4a. DCS, decorrelation stretch.

and 1.15 μm, phyllosilicate-bearing materials (Phy) appear red and orange, chloride-bearing materials (Chl) appear blue, and LCP-bearing materials appear green (Fig. 4a).

The ratioed CRISM reflectance spectra of representative color units are shown in Figure 4b and are color coded based on the typical unit color shown in Figure 4a. The ratioed spectra of both orange and red color units display prominent absorptions at 1.4, 1.9, and 2.3 μm, and a drop in reflectance at wavelengths greater than ~2.53 μm. The features at 1.4 and 1.9 μm are overtones of H_2O and OH^- molecules in the mineral structure, whereas 2.3 and 2.53 μm features indicate metal–OH vibrational overtones. These spectra are similar to a range of Fe- or Mg-rich smectites. The spectra of chlorides are characterized by a spectrally featureless red slope (increasing reflectance with increasing wavelength), which might be due to mixture of chloride and basaltic materials (Jensen and Glotch, 2011). The high values near 3.0 μm in ratioed spectra are indicative of dehydration in chlorides relative to typical silicate-bearing materials (Fig. 5). The spectrum of LCP-rich materials presents a broad 2 μm feature, consistent with an Fe^{2+} crystal field absorption (Burns, 1993).

The eroded alluvial fan and the related deposits lay in the lowest portion of the basin (Fig. 1), separated from the rest of the basin by a NE–SW scarp (Fig. 2a). All of the chlorides in the study area have blue hues (Fig. 6a, b) in the HiRISE

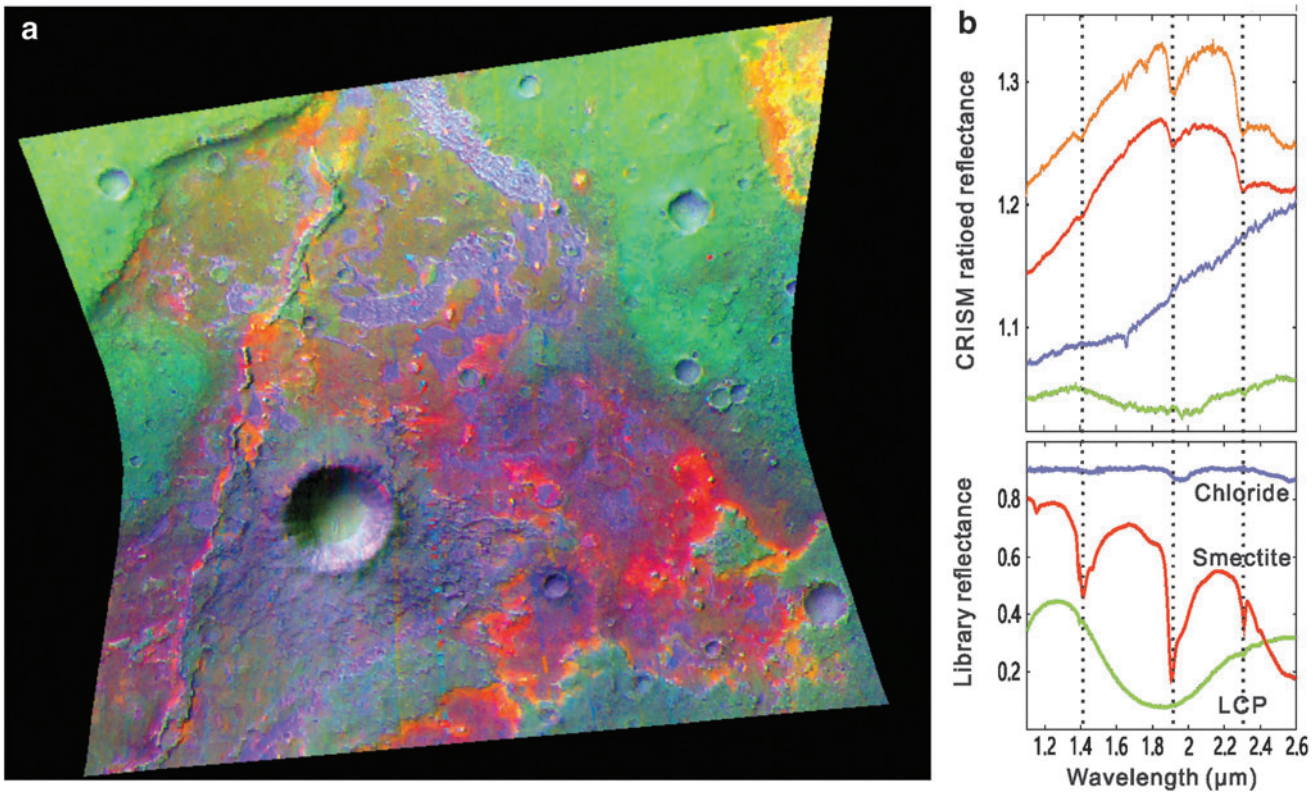

FIG. 4. **(a)** DCS of CRISM FRT0000B001 bands 1.8, 2.38, and 1.15 μm. This combination results in phyllosilicates appearing red and orange, chlorides appearing blue, and LCP appearing green; **(b)** ratioed CRISM spectra compared with library mineral reflectance spectra. Colors of the CRISM spectra correspond to colors in **(a)**. The library spectra are from the CRISM and USGS spectral libraries. CRISM, Compact Reconnaissance Imaging Spectrometer for Mars; LCP, low-calcium pyroxene.

color image (red: 900 nm, green: 700 nm, blue: 500 nm), which is common of chloride deposits (Osterloo *et al.*, 2010). Furthermore, based on our mapping of this unit at HiRISE scales, this unit appears to be a continuous layer throughout the region (Figs. 2a and 3a, b), despite being superposed by other units

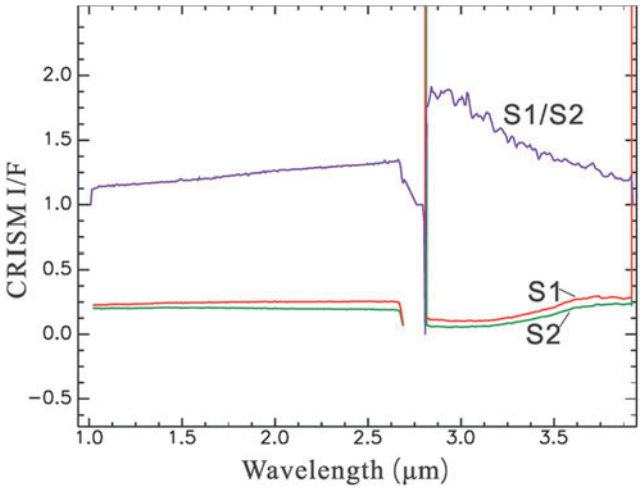

FIG. 5. An example of ratioed CRISM spectra of chlorides. The high values near 3.0 μm in ratioed spectra are indicative of dehydration in chlorides relative to typical silicate-bearing materials. S1 and S2 are average of 5×5 pixels centered at (274, 401) and (274, 371), respectively.

(ejecta, mounds, etc.). We observed polygonal fractures with widths of 1–2 m on the surface of the chlorides (Fig. 6b). The fractures are generally straight and they usually formed quadrangle shapes. Dark materials occurred in the fractures. Parallel ridges (Figs. 6a and 7a, c) stretch several 100 m. The symmetrical morphology and parallel orientation (Fig. 7c) indicate that they are aeolian in origin. CTX DEM measurements over different occurrences of the chlorides show that the thickness of the chlorides is tens of meters and variable throughout the region, whereas the phyllosilicate-bearing units display a polygonally fractured texture (Figs. 6b and 7b) and are meters thick.

Different materials with interesting stratigraphic relationships are revealed by CTX and HiRISE images and DTMs. At one location (Fig. 6b), chlorides occur in the lowest topographic regions in both the northern and southern portions, whereas outcrops of pyllosilicate-bearing materials occur at higher elevation comparing with the southern chlorides unit exposure (Fig. 6c). Possible aeolian deposits (Ad) compose an upper layer, and chlorides can be observed within erosional windows of the aeolian deposits (Fig. 6b). A dark-toned material with basaltic composition also occurs stratigraphically above the chloride-bearing materials and is present within the intercrest plains of chlorides (Fig. 7a). Some portions of the dark-toned materials have flow-like morphologies (Fig. 7a). Ridges of tens of meters in length can be observed in these materials, and these ridges may be an indication of an evaporate environment (Fig. 7a) based on the similar appearance of the ridges commonly observed

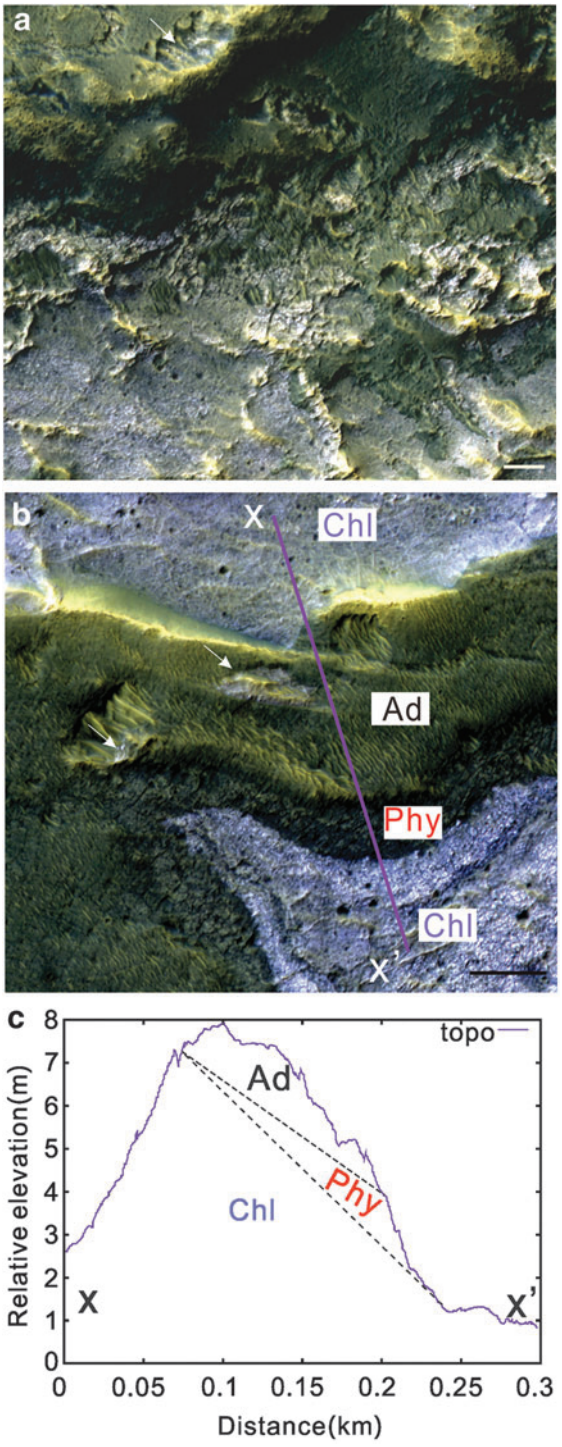

FIG. 6. **(a)** Eroded chloride-bearing materials appear to be in place and occur at different elevation near the SW–NE scarp (indicated by yellow arrows in Fig. 2a). The white arrow indicates an erosional ''window'' exposing chlorides; **(b)** chlorides (Chl) occurred in the lowest topographic areas. Phyllosilicates (Phy) are emplaced directly above the chlorides. Aeolian deposits (Ad) are on the top with erosional ''windows'' exposing chlorides indicated by white arrows; **(c)** relative elevation profile derived from HiRISE DTMs and potential stratigraphy along the line x–x′ in **(b)**. **(a, b)** are portion of color image of HiRISE PSP_008780_1735, and the scale bars are 50 m.

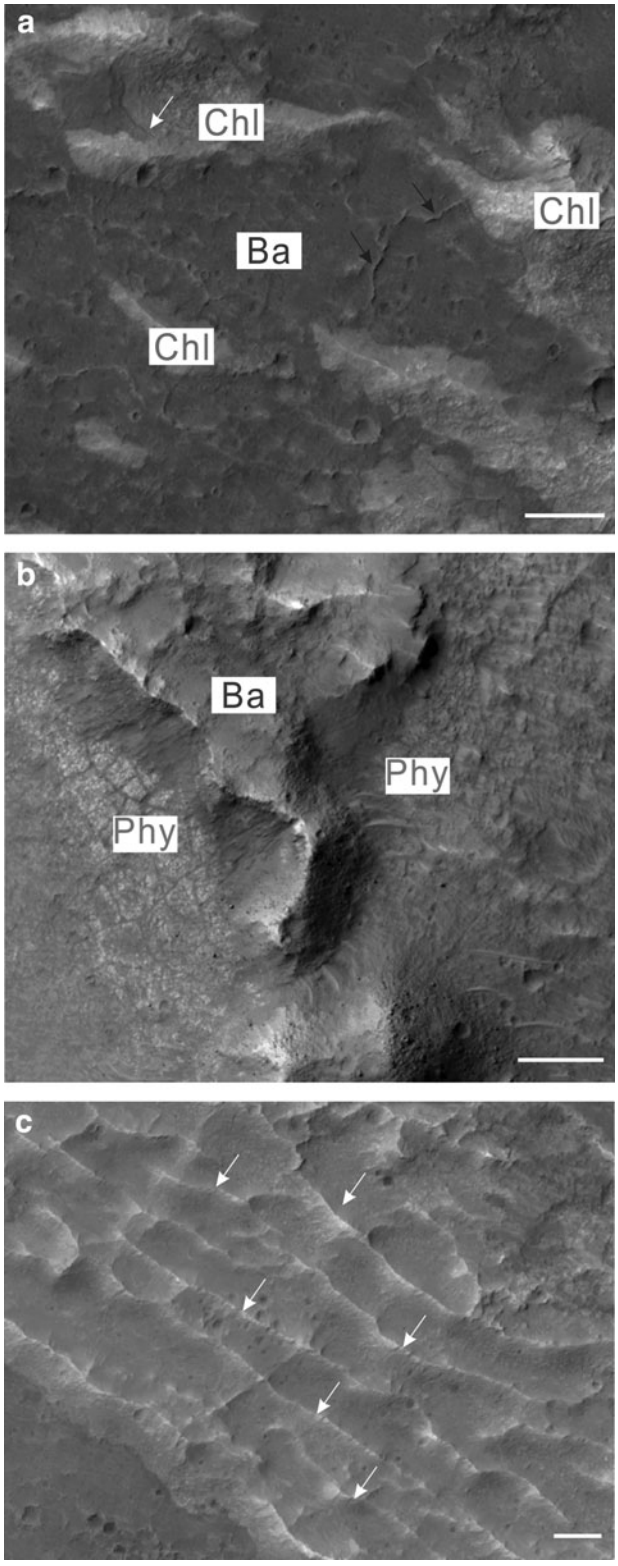

FIG. 7. **(a)** Dark-toned, thin layer of basaltic materials occurred in the intercrest plains of chlorides. The ridges pointed by arrows indicate evaporation due to the similarity of terrestrial counterparts; **(b)** phyllosilicates are stratigraphically below the remnants of the basaltic materials within the alluvial fan. HiRISE PSP_008780_1735, and the scale bars are 50 m; **(c)** white arrows indicate chloride ridges with parallel orientations and dune-like morphologies. Scale bars are 50 m in all panels.

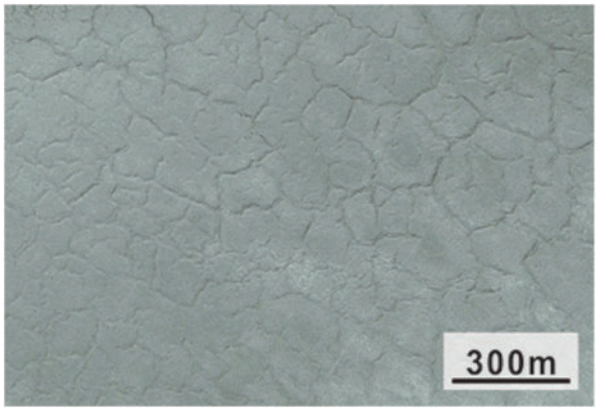

FIG. 8. Elevated ridges in playa in the Qaidam Basin, China (91.53°E, 38.40°N). On Earth, these features in the salt crust are interpreted to form by evaporation and crystallization of halite during the desiccation stage of the saline lake cycle.

in terrestrial playas (Fig. 8) (Lowenstein and Hardie, 1985; Xiao *et al.*, 2017). However, the detailed relationship between the dark-toned basaltic materials (Ba) relative to the phyllosilicate-bearing materials could not be determined with currently available data. A thick capping layer of unaltered basaltic materials (Fig. 6a) is observed above the chlorides, the phyllosilicates (Fig. 7b), and the thinner, dark-toned basaltic materials.

4. Discussion

Most of the ~640 chloride sites identified on Mars have been identified on terrains formed from the middle Noachian to the early Hesperian geological periods (Osterloo *et al.*, 2010), but absolute model ages of these chlorides are poorly constrained due to their small geographic extents for crater size–frequency distribution (CSFD) measurements. Therefore, the stratigraphic relationship of the chlorides and surrounding units is the primary means to constrain the timing of chloride formation. The basaltic materials of the valley floor, which are stratigraphically above the chlorides and large enough for CSFD measurements, could provide a lower limit of the formation time for these chlorides. Ehlmann and Buz (2015) have determined the absolute model age of the valley floor to be 3.7 Ga, indicating that the stratigraphically underlying chlorides formed earlier than 3.7 Ga, which corresponds to the late Noachian or the early Hesperian (Hartmann and Neukum, 2001).

Several hypotheses have been proposed to explain the formation of the chloride-bearing materials on the surface of Mars (Osterloo *et al.*, 2010): (1) precipitation in a body of water from surface runoff or groundwater upwelling; (2) impact or volcanic activity generated hydrothermal brine; and (3) fumarolic activity or atmospheric interactions generated efflorescence. In our study area, the diameters of all the impact craters are inferior to 2 km, therefore, these craters did not excavate deep enough or have enough kinetic energy to initiate hydrothermal activities. In addition, no morphological (fluidized ejecta or pedestal craters) or mineralogical (*e.g.*, sulfur or silica) pieces of evidence have been identified. Therefore, the second hypothesis is not likely the case. For the third hypothesis, we did not observe volcanic constructions or well-developed fractures or ''haloing.'' Instead, the chlorides identified in the study region occurred in topographic lows, and the adjacent region is carved by extensive fluvial channels. Furthermore, numerous polygonal fractures occurred in the chlorides. In sum, we prefer the chlorides in this study are most likely to be sediments from the precipitation of chloride from lakes, as previous studies have shown (Osterloo *et al.*, 2010; Ehlmann and Edwards, 2014; Hynek *et al.*, 2015), indicating surface water activity and evaporitic environments occurred contemporaneously. Although the origin of the phyllosilicate-bearing materials may be a result of *in situ* aqueous alteration of a basaltic precursor (Zolotov and Mironenko, 2016) as no obvious transport mechanisms are observed, it is possible the evidence of transportation has been erased as erosion of the overlying deposits occurred to expose the units observed today. However, evidence for the provenance of these phyllosilicate materials, if transported, has not been identified in a more reginal-scale search of CRISM data, where available.

One possible scenario for the formation of the observed geological units (Fig. 9) is that these chlorides formed from the evaporation of high-salinity water imported from the various infill channels and subsequent precipitation of dissolved chloride salts. Afterward, polygonal fractures formed in the chlorides due to desiccation (El-Maarry *et al.*, 2013,

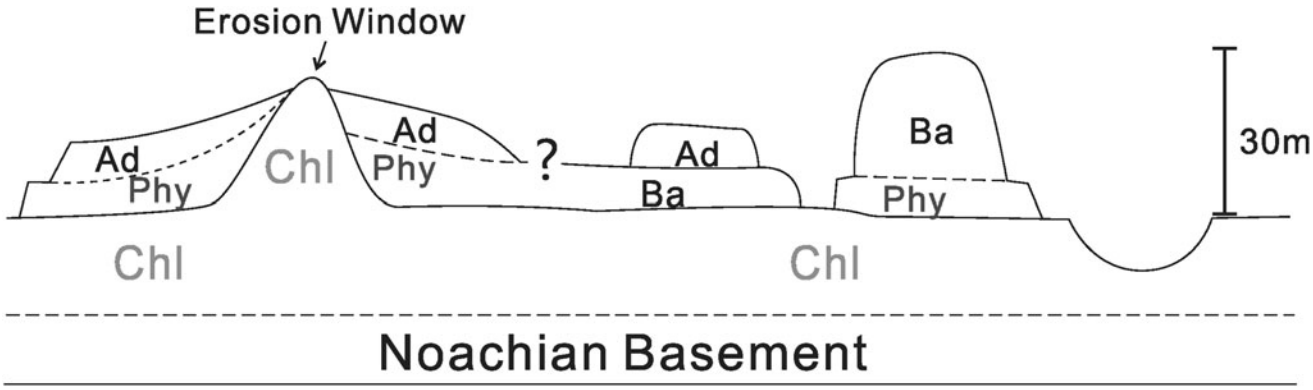

FIG. 9. Conceptual diagram showing one possible stratigraphic relationships between observed geological units (not to scale). Ad, aeolian deposits; Ba, basaltic materials; Chl, chlorides; Phy, phyllosilicates.

2014), and portions of these deposits likely underwent aeolian modification to form the observed ridges. A thin layer ($\sim$1–3 m) of basaltic material, possibly volcanic ash, was deposited on the chlorides. Highly fractured phyllosilicates observed in a portion of this basaltic layer may have formed by transportation or contemporaneous/subsequent *in situ* alteration (Zolotov and Mironeko, 2016). Continued fluvial activity resulted in the formation of an alluvial fan, superimposing the underlying chloride- and smectite-bearing deposits. The fan was later eroded by subsequent geological processes, potentially contributing to the overlying aeolian deposits that lie on top of all the in-place geological units.

However, an alternative explanation of chlorides contemporaneous with phyllosilicates (Milliken *et al.*, 2009) or relatively younger chlorides with older phyllosilicates cannot be ruled out due to lack of definitive stratigraphic observations (*e.g.*, stratigraphic exposures on walls of impact craters or canyons, well-preserved zoned impact crater ejecta). In this scenario, brine fluid accumulated in regional topographic low area after the deposition or *in situ* formation of phyllosilicate-bearing materials, and the chlorides formed through evaporation or upwelling. Therefore, the phyllosilicate-bearing materials could occur topographically higher but stratigraphically lower than the chlorides. Regardless of the precise stratigraphic relationship between the chlorides and phyllosicilate-bearing units, these two units are intimately connected. If the phyllosilicate alteration occurred after the precipitation of the chlorides, then the prevalence of playa could extend further into history than previously thought. However, if the phyllosilicates were transferred fluvially and deposited on top of the chlorides, it is likely that the chloride-bearing unit was at least subject to partial dissolution and reprecipitation. Importantly, such a sequence of events (rewetting of chloride-bearing units by other fluvial activity) likely results in the appearance of these units as some of the stratigraphically highest in their regions, leaving their original formation time unconstrained (although likely older than the latest fluvial event). This process could be responsible for the widespread appearance that the chlorides are relatively young in comparison with their surroundings, despite their potentially unknown original formation time. Furthermore, the enigmatic relationship of the chlorides and phyllosilicates observed here is unique among current observations and illustrates the complicated nature and timing of the hydrological cycle in early Mars history.

The juxtaposition of ancient chlorides with superimposed Fe–Mg-rich smectites offers unique astrobiological prospects in the search for potential martian biosignatures. If ancient Mars did host life, this old evaporitic fluviolacustrine setting may have remained habitable long after the rest of the surface became inhospitable. Fluvial deposits overlying evaporites suggest that redissolved solutes would have allowed liquid water to remain stable as the planet entered the Noachian–Hesperian climate transition (Brass, 1980; Clark and Van Hart, 1981; Haberle *et al.*, 2001; Burt and Knauth, 2003; Fairén, 2010). As smectites are prone to rapid (<1 year half-life) dissolution under acidic conditions (Rozalén *et al.*, 2008), the ubiquity of these deposits at the site supports their deposition in circumneutral pH waters.

Although liquid water may not have been stable for long periods at large scales, microscopic fluid inclusions present one possibility where liquid water could have persisted. Fluid inclusions in terrestrial evaporite deposits have preserved ancient aquatic chemistry and biosignatures, including metabolites, nucleic acids, and perhaps even viable microbial communities for hundreds of millions of years (Reiser and Tasch, 1960; Dombrowski, 1963; Norton *et al.*, 1993; Gemmell *et al.*, 1998; McGenity *et al.*, 2000; Vreeland *et al.*, 2000, 2007; Fish *et al.*, 2002; Stan-Lotter *et al.*, 2002; Ueno *et al.*, 2006; Schubert *et al.*, 2010; Saralov *et al.*, 2013). Dissolved salts in these inclusions also provide protection from ultraviolet radiation, which would threaten the preservation of organic matter on the present martian surface (Yopp *et al.*, 1979; Rothschild, 1990). Furthermore, the large mineralogical surface area and high cation exchange capacity of smectites render these phases very sorbent of organic matter from aqueous solutions relative to other phyllosilicate mineralogies (Eslinger and Pevear, 1988; Kennedy *et al.*, 2002; Qu *et al.*, 2011). Thus, smectite deposits at the site provide a potential role in carbon sequestration.

Even today, hygroscopic salts present in the chloride deposits may be subject to periodic deliquescence (Martín-Torres *et al.*, 2015), allowing for the formation of transient liquid brines. Davila *et al.* (2010) demonstrated that NaCl deposits could seasonally deliquesce under modern martian conditions, demonstrating water activities (a_w) supportive of microbial metabolism and growth, as defined by known temperature and a_w limits for life (Harris, 1981; Rivkina *et al.*, 2000; Price and Sowers, 2004). Following the lower temperature and a_w limits (−28°C and $a_w = 0.5$, respectively) used to define Mars special regions (Beaty *et al.*, 2006; Kminek and Rummel, 2015), Davila *et al.* (2010) also report that deliquescent $CaCl_2$ solutions may also support microbial activity and propagation. We postulate that smectite minerals immediately superjacent to chlorides at the site are well situated to sorb any potential organic matter from deliquesced brines, offering preservation potential against oxidative and photochemical dissociation. Evidence of ancient microbial activity may be indicated at larger scales in the form of microbially induced sedimentary structures (MISS) similar to endolithic salt crusts found in terrestrial deserts, including the driest region of the Atacama Desert (Wierzchos *et al.*, 2006) and in Antarctica Peninsula (Hughes and Lawley, 2003). Distinctive visual clues indicating microbial (as opposed to physical) inducement would include the presence of features such as wrinkles, pinnacles, and polygonal folding of the crust (Noffke *et al.*, 2001; Noffke, 2010). Although MISS can occur laterally across centimeter to kilometer-scale on Earth (Noffke, 2015), it will be possible but very challenging to identify MISS using orbital remote sensing data (even at HiRISE image resolution) due to submeter topographical relief of MISS. It will be critical for a future *in situ* mission to take photographs of potential MISS at different lighting conditions (Noffke, 2015) to have a better chance to get a sample with the greatest organic preservation potential in locations physically protected from wind erosion and ultraviolet radiation, whereas the aeolian deposits and unaltered basaltic materials can be selected as blank for comparison.

5. Conclusion

We have identified coexistence of chlorides and Fe–Mg-bearing smectites in a complex fluviolacustrine environment on early Mars. These chlorides likely formed from evaporation

of briny water in the late Noachian to early Hesperian, whereas the phyllosilicates formed from alteration of basaltic materials in subsequent fluvial deposition or they were formed elsewhere and subsequently transported to their current position. Several previous studies have identified clear strata that chlorides above phyllosilicates, but this study has shown a complex relationship between these two deposits and provided a possible scenario of old chlorides and younger phyllosilicates. The early formation time and complicated stratigraphic relationship of these deposits, along with intriguing astrobiogical potentials of chloride deposits, make this site or similar sites where phyllosilicates and chlorides are colocated, a high priority astrobiological location for future *in situ* exploration and sample return missions.

Acknowledgments

JMARS (jmars.asu.edu), CAT (pds-geosciences.wustl.edu/missions/mro/crism.htm), and Davinci (davinci.asu.edu) are used in data process. We appreciate the HiRISE team for acquiring the image ESP_044502_1735 for the DTM generation. Data can be accessed from pds.jpl.nasa.gov with IDs. We thank comments from Dr. J. Bandfield and Dr. B. Craddock. Formal reviews by three anonymous and Associate Editor Dr. Chris McKay greatly improved the quality of this article. J.H. was supported by National Scientific Foundation of China (Nos. 41403052 and 41773061), the Fundamental Research Funds for the Central Universities, China University of Geosciences (Wuhan) (Nos. CUGL160402 and CUG2017G02), MOST Special Fund from the State Key Laboratory of Geological Processes and Mineral Resources (No. MSFGPMR05) and Lunar and Planetary Science Laboratory, Macau University of Science and Technology–Partner Laboratory of Key Laboratory of Lunar and Deep Space Exploration, Chinese Academy of Sciences (FDCT No. 039/2013/A2). R.L.H. is supported by National Science Foundation grant DGE-1148900. This work was not affiliated with any NASA projects or funding.

Author Disclosure Statement

No competing financial interests exist.

References

Bandfield, J.L., Rogers, D., Smith, M.D., and Christensen, P.R. (2004) Atmospheric correction and surface spectral unit mapping using Thermal Emission Imaging System data. *J Geophys Res Planets* 109:E10.

Beaty, D., K.B., Meyer, M., Barlow, N., Boynton, W., Clark, B., Deming, J., Doran, P.T., Edgett, K., Hancock, S., Head, J., Hecht, M., Hipkin, V., Kieft, T., Mancinelli, R., McDonald, E., McKay, C., Mellon, M., Newsom, H., Ori, G., Paige, D., Schuerger, A.C., Sogin, M., Spry, J.A., Steele, A., Tanaka, K., and Voytek, M. (2006) Findings of the Mars Special Regions Science Analysis Group. *Astrobiology* 6:677–732.

Brass, G.W. (1980) Stability of Brine on Mars. *Icarus* 42:20–28.

Burns, R.G. (1993) *Mineralogical Applications of Crystal Field Theory*. Cambridge University Press, New York.

Burt, D.M. and Knauth, L.P. (2003) Electrically conducting, Ca-rich brines, rather than water, expected in the Martian subsurface. *J Geophys Res Planets* 108:E4.

Christensen, P.R., Bandfield, J.L., Hamilton, V.E., Ruff, S.W., Kieffer, H.H., Titus, T.N., Malin, M.C., Morris, R.V., Lane, M.D., Clark, R.L., Jakosky, B.M., Mellon, M.T., Pearl, J.C., Conrath, B.J., Smith, M.D., Clancy, R.T., Kuzmin, R.O., Roush, T., Mehall, G.L., Gorelick, N., Bender, K., Murray, K., Dason, S., Greene, E., Silverman, S., and Greenfield, M. (2001) Mars global surveyor thermal emission spectrometer experiment: investigation description and surface science results. *J Geophys Res Planets* 106:23823–23871.

Christensen, P.R., Jakosky, B., Kieffer, H.H., Malin, M.C., McSween, H.Y., Nealson, K., Mehall, G.L., Silverman, S.H., Ferry, S., Caplinger, M., and Ravine, M. (2004) The Thermal Emission Imaging System (THEMIS) for the Mars 2001 Odyssey Mission. *Space Sci Rev* 10:85–130.

Clark, B.C. and Van Hart, D.C. (1981) The salts of Mars. *Icarus* 45:370–378.

Davila, A.F., Duport, L.G., Melchiorri, R., Jänchen, J., Valea, S., de Los Rios, A., Fairén, A.G., Möhlmann, D., McKay, C.P., Ascaso, C., and Wierzchos, J. (2010) Hygroscopic salts and the potential for life on Mars. *Astrobiology* 10:617–628.

Dombrowski, H. (1963) Bacteria from Paleozoic salt deposits. *Ann N Y Acad Sci* 108:453–460.

Edwards, C.S., Bandfield, J.L., Christensen, P.R., and Fergason, R.L. (2009) Global distribution of bedrock exposures on Mars using THEMIS high-resolution thermal inertia. *J Geophys Res* 114, doi:10.1029/2009je003363.

Edwards, C.S., Christensen, P.R., and Hill, J. (2011) Mosaicking of global planetary image datasets: 2. Modeling of wind streak thicknesses observed in Thermal Emission Imaging System (THEMIS) daytime and nighttime infrared data. *J Geophys Res Planets* 116:E10.

Ehlmann, B.L. and Buz, J. (2015) Mineralogy and fluvial history of the watersheds of Gale, Knobel, and Sharp craters: a regional context for the Mars Science Laboratory Curiosity's exploration. *Geophys Res Lett* 42:264–273.

Ehlmann, B.L. and Edwards, C.S. (2014) Mineralogy of the martian surface. *Annu Rev Earth Planet Sci* 42:291–315.

Ehlmann, B.L., Mustard, J.F., Fassett, C.I., Schon, S.C., Head, J.W., III, Des Marais, D.J., Grant, J.A., and Murchie, S.L. (2008) Clay minerals in delta deposits and organic preservation potential on Mars. *Nat Geosci* 1:355–358.

El-Maarry, M.R., Pommerol, A., and Thomas, N. (2013) Analysis of polygonal cracking patterns in chloride-bearing terrains on Mars: indicators of ancient playa settings. *J Geophys Res Planets* 118:2263–2278.

El-Maarry, M.R., Watters, W., McKeown, N.K., Carter, J., Noe Dobrea, E., Bishop, J.L., Pommerol, A., and Thomas, N. (2014) Potential desiccation cracks on Mars: a synthesis from modeling, analogue-field studies, and global observations. *Icarus* 241:248–268.

Eslinger, E. and Pevear, D.R. (1988) Clay Minerals for Petroleum Geologists and Engineers (No. 22). Sepm Society for Sedimentary.

Fairén, A.G. (2010) A cold and wet Mars. *Icarus* 208:165–175.

Farmer, J.D. and Des Marais, D.J. (1999) Exploring for a record of ancient Martian life: *J Geophys Res Planets* 104:26977–26995.

Fergason, R.L., Christensen, P.R., and Kieffer, H.H. (2006) High-resolution thermal inertia derived from the Thermal Emission Imaging System (THEMIS): thermal model and applications. *J Geophys Res* 111:E12.

Fish, S.A., Shepherd, T.J., McGenity, T.J., Grant, W.D. (2002) Recovery of 16S ribosomal RNA gene fragments from ancient halite. *Nature* 417:432–436.

Gemmell, R.T., McGenity, T.J., and Grant, W.D. (1998) Use of molecular techniques to investigate possible long-term dormancy of halobacteria in ancient halite deposits. *Anc Biomol* 2:123–133.

Gillespie, A.R., Kahle, A.B., and Walker, R.E. (1986) Color enhancement of highly correlated images. 1. decorrelation and HSI contrast stretches. *Remote Sens Environ* 20:209–235.

Glotch, T.D., Bandfield, J.L., Tornabene, L.L., Jensen, H.B., and Seelos, F.P. (2010) Distribution and formation of chlorides and phyllosilicates in Terra Sirenum, Mars. *Geophys Res Lett* 37: L16202.

Glotch, T.D., Bandfield, J.L., Wolff, M.J., Arnold, J.A., and Che, C. (2016) Constraints on the composition and particle size of chloride salt-bearing deposits on Mars. *J Geophys Res Planets* 121:454–471.

Haberle, R.M., McKay, C.P., Schaeffer, J., Cabrol, N.A., Grin, E.A., Zent, A.P., and Quinn, R. (2001) On the possibility of liquid water on present day Mars. *J Geophys Res* 106:23317–23326.

Harris, R.F. (1981) Effect of water potential on microbial growth and activity. *Water Potential Relations in Soil Microbiology*, (waterpotential), pp 23–95.

Hartmann, W.K. and Neukum, G. (2001) Cratering chronology and the evolution of Mars. *Space Sci Rev* 96:165–194.

Huang, J., Edwards, C.S., Ruff, S.W., Christensen, P.R., and Xiao, L. (2013) A new method for the semiquantitative determination of major rock-forming minerals with thermal infrared multispectral data: application to THEMIS infrared data. *J Geophys Res Planets* 118:7.

Hughes, K.A. and Lawley, B. (2003) A novel Antarctic microbial endolithic community within gypsum salts. *Environ Microbiol* 5:555–565.

Hynek, B.M., Osterloo, M.K., and Kierein-Young, K.S. (2015) Late-stage formation of Martian chloride salts through ponding and evaporation. *Geology* 43:G36895.1.

Jensen, H.B. and Glotch, T.D. (2011) Investigation of the near-infrared spectral character of putative Martian chloride deposits. *J Geophys Res Planets* 16:E00J03.

Kennedy, M.J., Pevear, D.R., and Hill, R.J. (2002) Mineral surface control of organic carbon in black shale. *Science* 295: 657–660.

Kieffer, H.H. (2013) Thermal model for analysis of Mars infrared mapping. *J Geophys Res Planets* 118:451–470.

Kieffer, H.H., Martin, T.Z., Peterfreund, A.R., Jakosky, B.M., Miner, E.D., and Palluconi, F.D. (1977) Thermal and albedo mapping of Mars during the Viking Primary Mission. *J Geophys Res* 82:4249–4291.

Kminek, G. and Rummel, J.D. (2015) Planetary Protection Policy. *Space Res Today* 193:7–19.

Lowenstein, T.K. and Hardie, L.A. (1985) Criteria for the recognition of salt-pan evaporites. *Sedimentology* 3:627–644.

Malin, M.C., Bell, J.F., Cantor, B.A., Caplinger, M.A., Calvin, W.M., Clancy, R.T., Edgett, K.S., Edwards, L., Haberle, R.M., James, P.B., Lee, S.W., Ravine, M.A., Thomas, P.C., and Wolff, M.J. (2007) Context Camera Investigation on board the Mars Reconnaissance Orbiter. *J Geophys Res Planets* 112:E5.

Martín-Torres, F.J., Zorzano, M.-P., Valentín-Serrano, P., Harri, A.-M., Genzer, M., Kemppinen, O., Rivera-Valentin, E.G., Jun, I., Wray, J., Bo Madsen, M., Goetz, W., McEwen, A.S., Hardgrove, C., Renno, N., Chevrier, V.F., Mischna, M., Navarro-González, R., Martínez-Frías, J., Conrad, P., McConnochie, T., Cockell, C., Berger, G., Vasavada, A.R., Sumner, D., and Vaniman, D. (2015) Transient liquid water and water activity at Gale crater on Mars. *Nat Geosci* 8:357–361(E5).

McEwen, A.S., Eliason, E.M., Bergstrom, J.W., Bridges, N.T., Hansen, C.J., Delamere, W.A., Grant, J.A., Gulick, V.C., Herkenhoff, K.E., Keszthelyi, L., Kirk, R.L., Mellon, M.T., Squyres, S.W., Thomas, N., and Weitz, C.M. (2007) Mars Reconnaissance Orbiter's High Resolution Imaging Science Experiment (HiRISE). *J Geophys Res Planets* 112:E5.

McGenity, T.J., Gemmell, R.T., Grant, W.D., and Stan-Lotter, H. (2000) Origins of halophilic microorganisms in ancient salt deposits. *Environ Microbiol* 2:243–250.

McGuire, P.C., Bishop, J.L., Brown, A.J., Fraeman, A.A., Marzo, G.A., Frank Morgan, M., Murchie, S.L., Mustard, J.F., Parente, M., Pelkey, S.M., Roush, T.L., Seelos, F.P., Smith, M.D., Wendt, L., and Wolff, M.J. (2009) An improvement to the volcano-scan algorithm for atmospheric correction of CRISM and OMEGA spectral data. *Planet Space Sci* 57:809–815.

Mellon, M.T., Jakosky, B.M., Kieffer, H.H., and Christensen, P.R. (2000) High-resolution thermal inertia mapping from the Mars Global Surveyor Thermal Emission Spectrometer. *Icarus* 148:437–455.

Milliken, R.E., Fischer, W.W., and Hurowitz, J.A. (2009) Missing salts on early Mars. *Geophys Res Lett* 36:11:L11202.

Murchie, S., Arvidson, R., Bedini, P., Beisser, K., Bibring, J. P., Bishop, J., Boldt, J., Cavender, P., Choo, T., Clancy, R.T., Darlington, E.H., Marais, D.D., Espiritu, R., Fort, D., Green, R., Guinness, E., Hayes, J., Hash, C., Heffernan, K., Hemmler, J., Heyler, G., Humm, D., Hutcheson, J., Izenberg, N., Lee, R., Lees, J., Lohr, D., Malaret, E., Martin, T., McGovern, J.A., McGuire, P., Morris, R., Mustard, J., Pelkey, S., Rhodes, E., Robinson, M., Roush, T., Schaefer, E., Seagrave, G., Seelos, F., Silverglate, P., Slavney, S., Smith, M., Shyong, W.J., Strohbehn, K., Taylor, H., Thompson, P., Tossman, B., Wirzburger, M., and Wolff, M. (2007) Compact Reconnaissance Imaging Spectrometer for Mars (CRISM) on Mars Reconnaissance Orbiter (MRO). *J Geophys Res Planets* 112:E5.

Murchie, S.L., Mustard, J.F., Ehlmann, B.L., Milliken, R.E., Bishop, J.L., McKeown, N.K., Noe Dobrea, E.Z., Seelos, F.P., Buczkowski, D.L., Wiseman, S.M., Arvidson, R.E., Wray, J.J., Swayze, G., Clark, R.N., Des Marais, D.J., McEwen, A.S., and Bibring, J.-P. (2009) A synthesis of Martian aqueous mineralogy after 1 Mars year of observations from the Mars Reconnaissance Orbiter. *J Geophys Res Planets* 114:E2.

Noffke, N. (2010) *Microbial Mats in Sandy Deposits from the Archean Era to Today 194*. Berlin, Heidelberg: Springer-Verlag.

Noffke, N. (2015) Ancient sedimentary structures in the <3.7 Ga Gillespie Lake Member, Mars, that resemble macroscopic morphology, spatial associations, and temporal succession in terrestrial microbialites. *Astrobiology* 15:169–192.

Noffke, N., Gerdes, G., Klenke, T., and Krumbein, W.E. (2001) Microbially induced sedimentary structures—a new category within the classification of primary sedimentary structures: PERSPECTIVES. *J Sediment Res* 71:649–656.

Norton, C.F., McGenity, T.J., and Grant, W.D. (1993) Archaeal halophiles (halobacteria) from two British salt mines. *J Gen Microbiol* 139:1077–1081.

Osterloo, M.M., Hamilton, V.E., Bandfield, J.L., Glotch, T.D., Baldridge, A.M., Christensen, P.R., Tornabene, L.L., and Anderson, F.S. (2008) Chloride-bearing materials in the southern highlands of Mars. *Science* 319:1651–1654.

Osterloo, M.M., Anderson, F.S., Hamilton, V.E., and Hynek, B.M. (2010) Geologic context of proposed chloride-bearing materials on Mars. *J Geophys Res Planets* 115:E10.

Piqueux, S. and Christensen, P.R. (2011) Temperature-dependent thermal inertia of homogeneous Martian regolith. *J Geophys Res Planets* 116:E7.

Price, P.B. and Sowers T. (2004) Temperature dependence of metabolic rates for microbial growth, maintenance, and survival. *Proc Natl Acad Sci U S A* 101:4631–4636.

Putzig, N.E., Mellon, M.T., Kretke, K.A., and Arvidson, R.E. (2005) Global thermal inertia and surface properties of Mars from the MGS mapping mission. *Icarus* 173:325–341.

Qu, X., Zhang, Y., Li, H., Zheng, S., and Zhu, D. (2011) Probing the specific sorption sites on montmorillonite using nitroaromatic compounds and hexafluorobenzene. *Environ Sci Technol* 45:2209–2216.

Reiser, R. and Tasch, P. (1960) Investigation of the viability of osmophile bacteria of great geological age. *Trans Kans Acad Sci* 63:31–34.

Rivkina, E.M., Friedmann, E.I., McKay, C.P., and Gilichinsky, D.A. (2000) Metabolic activity of Permafrost Bacteria below the freezing point. *Appl Environ Microbiol* 66:3230–3233.

Rothschild, L.J. (1990) Earth anologs for martian life. Microbes in evaporites, a new model system for life on Mars. *Icarus* 88: 246–260.

Rozalén, M.L., Huertas, F.J., Brady, P.V., Cama, J., García-Palma, S., and Linares, J. (2008) Experimental study of the effect of pH on the kinetics of montmorillonite dissolution at 25 C. *Geochimica et Cosmochimica Acta* 72:4224–4253.

Ruesch, O., Poulet, F., Vincendon, M., Bibring, J.-P., Carter, J., Erkeling, G., Gondet, B., Hiesinger, H., Ody, A., and Reiss, D. (2012) Compositional investigation of the proposed chloride-bearing materials on Mars using near-infrared orbital data from OMEGA/MEx. *J Geophys Res Planets* 117:E00J13.

Saralov, A.I., Baslerov, R.V., and Kuznetsov, B.B. (2013) Haloferax chudinovii sp. nov., a halophilic archaeon from Permian potassium salt depoits. *Extremophiles* 17:499–504.

Schubert, B.A., Lowenstein, T.K., Timofeeff, M.N., and Parker, M.A. (2010) Halophilic Archaea cultured from ancient halite, Death Valley, California: *Environ Microbiol* 12:440–454.

Shean, D.E., Alexandrov, O., Moratto, Z.M., Smith, B.E., Joughin, I.R., Porter, C., and Morin, P. (2016) An automated, open-source pipeline for mass production of digital elevation models (DEMs) from very-high-resolution commercial stereo satellite imagery. *ISPRS J Photogramm Remote Sens* 116:101–117.

Stan-Lotter, H., Pfaffenhuemer, M., Legat, A., Busse, H.J., Radax, C, and Gruber, C. (2002) Halococcus dombrowskii sp. nov., an archaeal isolate from a Permo-triassic alpine salt deposit. *Int J Syst Evol Biol* 52:1807–1814.

Tanaka, K.L., Skinner, J.A., Dohm, J.M., Irwin, R.P., Kolb, E.J., Fortezzo, C.M., Platz, T., Michael, G.G., and Hare, T.M. (2014) *Geologic Map of Mars.* Geological Survey Scientific Investigations Map 3292, scale 1:20,000,000.

Ueno, Y., Yamada, K., Yoshida, N., Maruyama, S., and Isozaki, Y. (2006) Evidence from fluid inclusions for microbial methanogenesis in the early Archaean era. *Nature* 440:516–519.

Vreeland, R.H., Rosenzweig, W.D., and Powers, D.W. (2000) Isolation of 250 million-year-old halotolerant bacterium from a primary salt crystal *Nature* 407:897–900.

Vreeland, R.H., Jones, J., Monson, A., Rosenzweig, W.D., Lowenstein, T.K., Timofeeff, M., Satterfield, C., Cho, B.C., Park, J.S., Wallace, A., and Grant, W.D. (2007) Isolation of live Cretaceous (121–112 million years old) halophilic Archaea from primary salt crystals. *Geomicrobiol J* 24:275–282.

Wierzchos J., Ascaso C., and McKay C.P. (2006) Endolithic cyanobacteria in halite rocks from the hyperarid core of the Atacama Desert. *Astrobiology* 6:415–422.

Xiao, L., Wang J., Dang Y., Cheng Z., Huang T., Zhao J., Xu Y., Huang J., Xiao Z., and Komatsu G. (2017) A new terrestrial analogue site for Mars research: the Qaidam Basin, Tibetan Plateau (NW China). *Earth Sci Rev* 164:84–101.

Yopp, J. H., Albright, G., and Miller, D. M. (1979) Effects of antibiotics and ultraviolet radiation on the halophilic blue-green alga, Aphanothece halophytica: Botanica. *Marina* 22: 267–272.

Zolotov, M.Y., and Mironenko, M.V. (2016) Chemical models for martian weathering profiles: insights into formation of layered phyllosilicate and sulfate deposits. *Icarus* 275:203–220.

Address correspondence to:
Jun Huang
Planetary Science Institute
State Key Laboratory of Geological Processes and Mineral Resources
School of Earth Sciences
China University of Geosciences
Wuhan 430074
China

E-mail: junhuang@cug.edu.cn

Submitted 5 September 2017
Accepted 27 January 2018

Abbreviations Used

CAT = CRISM Analysis Tool
CRISM = Compact Reconnaissance Imaging Spectrometer for Mars
CSFD = crater size–frequency distribution
CTX = Context Camera
DCSs = decorrelation stretches
FRT = full resolution targeted
HiRISE = High Resolution Imaging Science Experiment
IR = infrared
JMARS = Java Mission-planning and Analysis for Remote Sensing
LCP = low-calcium pyroxene
MISS = microbially induced sedimentary structures
TES = Thermal Emission Spectrometer
THEMIS = Thermal Emission Imaging System